Check for updates

The Blasingame method considering the effect of inter-well interference in a circular homogeneous closed reservoir

Pengfei Du[1], Qi Wang[2], Jing Zhang[2], Yanwei Wang[1], Dong Wang[1], Yi Han[1] and Pengcheng Liu[1]*

[1]School of Energy Resources, China University of Geosciences, Beijing, China, [2]Research Institute of Petroleum Exploration and Development of CNPC, Beijing, China
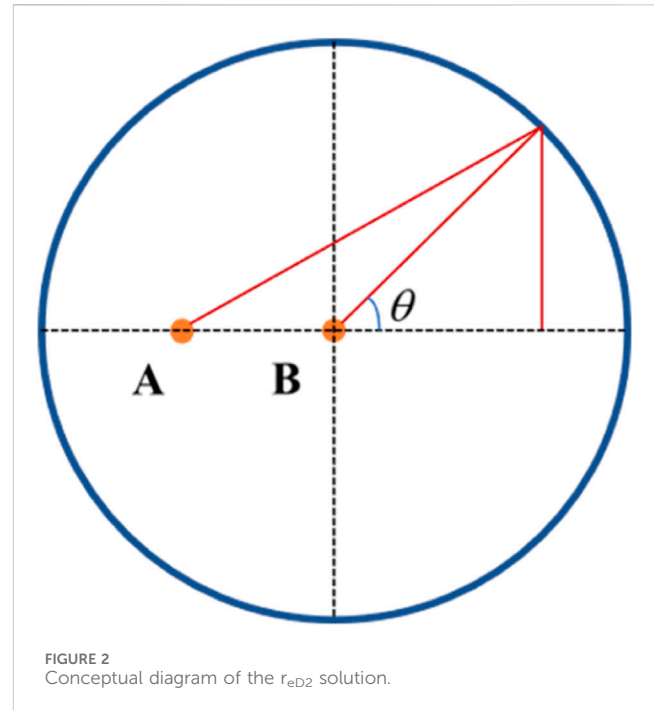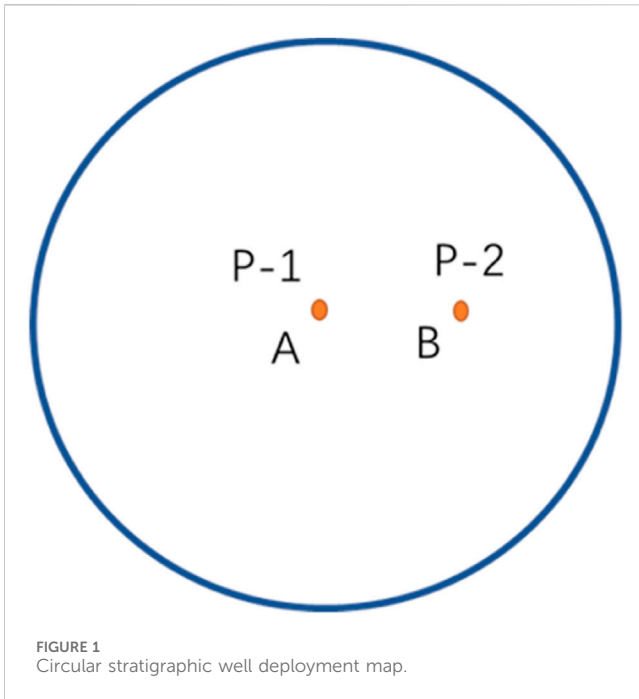
The Blasingame method is a valuable tool for analysing the diminishing production challenge in the presence of variable bottomhole pressure and diverse production conditions. It is essential to highlight that the Blasingame method views the closed reservoir as the outer boundary condition for its model. This paper introduces the concept of the equivalent well control radius and formulates the Blasingame method based on the fluid flow characteristics inherent in twin-well production, taking into account the influence of inter-well interference. This study provides an in-depth analysis of production variations in reservoirs with inter-well interference by examining Blasingame type-curve definitions of the dimensionless parameters. Additionally, it investigates key factors impacting production, including neighbouring wells' production, distance, and opening time: variations in all three parameters lead to different levels of interference between wells, which manifests itself in the regularised production integral derivative curve with different lengths and heights of convexity. Numerical simulations employing orthogonality are conducted to validate the reliability of this method. The results of these simulations offer theoretical support for the precise evaluation of reservoirs facing similar challenges.

KEYWORDS

twin-well production, mobile phase, equivalent well control radius, Blasingame-type curves, declining yield curve, explanatory plate

1 Introduction

In reservoirs with strong inter-well connectivity, neighbouring well interference can significantly impact test well pressures during the declining development process (Yuan and Wang, 2013; Guo et al., 2022; Wang et al., 2023). It has been well-established that reservoir dynamic description techniques, centred on single-well test well analysis and modern declining production analysis techniques, are effectively applied in reservoirs characterised by small single-well control ranges and poor inter-well connectivity (Zhang, 2004). However, reservoirs with high permeability and good connectivity are often multi-well systems (Zhang et al., 2006; Lin and Yang, 2007; Li and Luo, 2009). Therefore, interpreting such reservoirs using a single-well dynamic description can be

FIGURE 1
Circular stratigraphic well deployment map.

FIGURE 2
Conceptual diagram of the r_{eD2} solution.

misleading (Pang et al., 2012; Gan et al., 2022; Wang et al., 2023). Currently, the industry typically employs the superposition principle method to study the dynamic information of test wells in a multi-well system with inter-well interference (Onur et al., 1991; Li et al., 1994; Zhou et al., 2022). Jiaen Lin, Qiguo Liu, and Yonglu Jia demonstrated the late 'upward curvature' of the pressure recovery derivative curve in test wells by using the well test analysis technique (Dong and Zhai, 1996; Lin et al., 1996; Liu et al., 2002; Lin and Yang, 2005b; Liu et al., 2006; Jia et al., 2008; Deng et al., 2015). Hedong Sun provided a theoretical proof of this phenomenon while establishing an analysis method for multi-well pressure recovery test wells under neighbouring well interference conditions (Sun, 2016; Alarji. H et al., 2022). With the deepening of research, many scholars have explored the multi-well production model under the influence of multiple factors. Zeng Yang established a model for interpreting well tests in injection wells that consider interference from neighbouring wells (Zeng Y et al., 2020; Zhao et al., 2022). Cao established a well test interpretation model for finite inflow fractured wells under multi-well interference (Wei et al., 2022b).

The analytical solution of the multi-well production model discussed in previous studies is primarily used for analysing test wells (Jiang et al., 2019; Chen, 2023). The model assumes an infinite reservoir as the outer boundary condition, which simplifies the analysis. This paper introduces a closed reservoir as the outer boundary condition, introduces the 'normalisation factor', and applies the model's solution to the Blasingame-type curves (Chen et al., 2017; Xu et al., 2021).

Modern methods of diminishing yield analysis and well test analysis are based on the classical seepage basis, but the two methods use different accuracy of evaluation data in the analysis process (Sun, 2013; Spivey, 2016; Wei et al., 2022a). Modern methods of diminishing yield analysis require less precision in the data and are, therefore, less difficult and costly to obtain. Blasingame and others creatively introduced the proposed time of material equilibrium and regularised yields to establish a plate of decreasing curves called the Blasingame plate (Mccray, T.L, 1990; Palacio and Blasingame, 1993). It is epoch-making in the modern analysis of diminishing yield.

2 Modelling and solving

Figure 1 shows a circular stratigraphic well deployment map.

From Figure 1, the middle point of a circular formation with supply radius r_e and closed outer boundary, there is a well P-1 producing at a constant yield qi, while at point B, there is another well P-2 producing at a yield q_2, and the distance from point A to point B is L.

Other assumptions are as follows: the reservoir is homogeneous and isotropic, with impermeable boundaries above and below; the reservoir pores are filled with a single-phase, micro-compressible fluid, and the flow is in accordance with Darcy's law; the effect of gravity is neglected; and the effects of the skin effect and the wellbore storage effect are not considered.

2.1 Equivalent well control radius

The pull-down spatial pressure solution for point A of the double-well production, Eq. 1, can be obtained according to the Duhamel superposition principle (Wang, 2015):

$$\tilde{P}_A = \tilde{P}_{1A} + \tilde{P}_{2A}, \tag{1}$$

where $\tilde{P}_A$ is the pressure solution at point A when both wells are producing, $\tilde{P}_{1A}$ is the pressure solution at point A when well P-1 is producing alone, and $\tilde{P}_{2A}$ is the pressure solution at point A when well P-2 is producing alone.

TABLE 1 Equivalent well control radius error rating table.

Uncalculated well control radius (r_{eD})	Uncalculated well spacing (r_1)	Simplified unfactored well control radius (r_{eD2}) (results retained to four significant figures)	Ratio of the actual well control area to simplified well control area $\left(\frac{r_{eD}^2 \pi}{r_{eD2}^2 \pi} \right)$ (Results retained in three dimensions)
5,000	10	5,000	1.000
5,000	100	5,005	0.998
5,000	1,000	5,050	0.9803
5,000	2,000	5,198	0.9253
5,000	2,500	5,307	0.8877
5,000	3,000	5,438	0.8454
5,000	4,000	5,759	0.7537

FIGURE 3
Comparison of fixed production pressure inverse, fixed production output, and fixed production material balance time output curves **(A)**. q$_D$, 1/p$_D$ vs. t$_D$ curve; **(B)**. q$_D$ and 1/p$_D$ vs. t$_D$, q$_D$ vs. t$_{cD}$ curve (Hedong Sun, 2015).
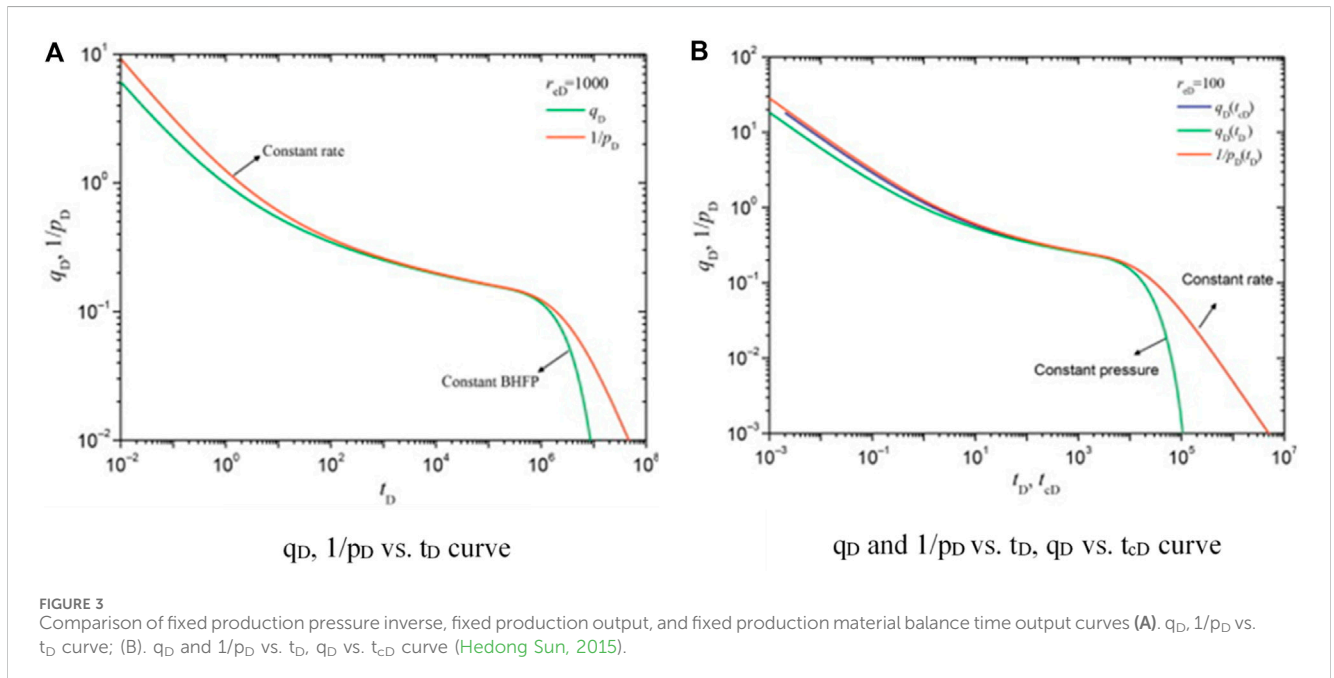
When L tends to 0, the pressure response of the unsteady seepage stage at point A is equivalent to the pressure response of well P-1 when it produces individually at a constant production rate ($q_i + q_2$), and the unsteady flow stage exhibits radial flow characteristics. When L is large, $q_i = q_2$, and $\tilde{P}_{1A} > \tilde{P}_{2A}$, the flow characteristics of the unstable seepage stage at point A are dominated by the flow characteristics of the unstable seepage stage at point A when well P-1 is producing alone.

Figure 2 shows a conceptual diagram of the r_{eD2} solution. Overall, in Figure 2, the flow stage at point A, when the two wells are producing, can be simplified as the infinite radial flow stage, the proposed steady-state stage. In turn, the pressure solution at point A when well P-2 is producing alone can be simplified as the pressure solution for one well in the centre of a circular closed reservoir with constant production, while the simplified well control radius expression for well B is given in this paper.

The average of the distances from point B to the circular closure boundary at the simplified drain radius is as follows:

$$r_{eD2} = \frac{\int_0^{2\pi} \left[(r_{eD} \sin \theta)^2 + (r_{eD} \cos \theta + r_1)^2 \right] d\theta}{2\pi}, \tag{2}$$

$$r_1 = \frac{L}{r_w}, \tag{3}$$

$$r_{eD} = \frac{r_e}{r_w}, \tag{4}$$

where r_{eD} is the radius of the circular closed reservoir and r_w is the radius of the wellbore.

From Eqs 2–4, we can derive ($r_{eD2} \geq r_{eD}$) (take the equal sign when L = 0), so the reservoir reaches the proposed steady-state flow stage later when P-2 is producing alone than when well P-1 is producing alone, which is in line with the actual flow condition.
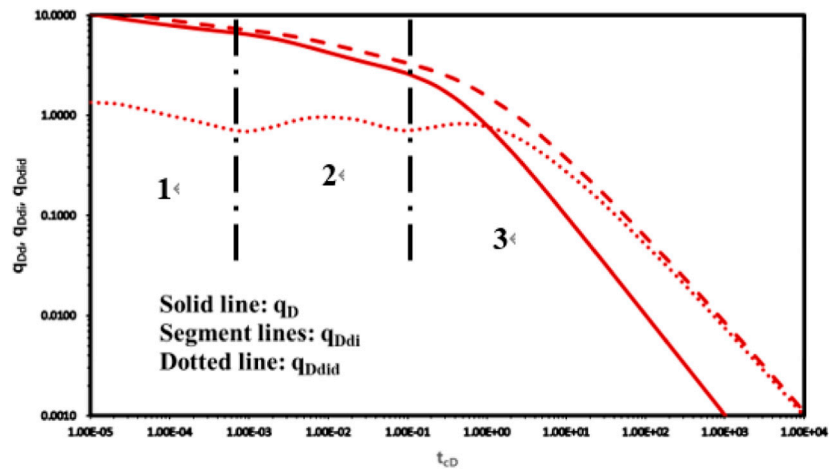
FIGURE 4
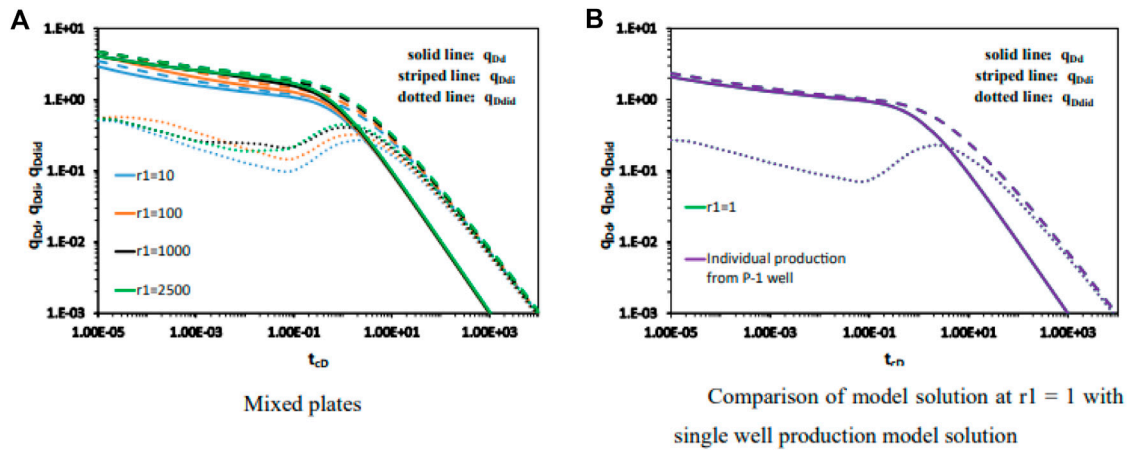Unstable analysis curve of production from double straight wells in homogeneous reservoirs.

FIGURE 5
Effect of different distances between two wells on the Blasingame curve when two wells in a circular homogeneous confined reservoir are producing at the same rate with simultaneous fixed production **(A)** Mixed plates; **(B)** Comparison of model solution at r1=1 with single well production model solution.

Table 1 lists the equivalent well control radius error rating table. After obtaining the simplified well control radius using this method, the corresponding equivalent well control area is further calculated and compared with the actual well control area. It is found that the simplified well control area is more accurate at $(r_1 < 0.5 r_{eD})$.

2.2 Modelling

The fixed solution problem for p-1 wells can be described as follows:

$$\frac{\partial^2 p_D}{\partial r_D^2} + \frac{1}{r_D} \frac{\partial p_D}{\partial r_D} = \frac{\partial p_D}{\partial t_D}, \tag{5}$$

$$p_D\big|_{t_D=0} = 0, \tag{6}$$

$$r_D \frac{\partial p_D}{\partial r_D}\bigg|_{r_D=1} = -1, \tag{7}$$

$$\frac{\partial p_D}{\partial r_D}\bigg|_{r_D=r_{eD}} = 0, \tag{8}$$

$$p_{1A} = p_D(1, t_D). \tag{9}$$

The fixed solution problem for p-2 wells can be described as follows:

$$\frac{\partial^2 p_D}{\partial r_D^2} + \frac{1}{r_D} \frac{\partial p_D}{\partial r_D} = \frac{\partial p_D}{\partial t_D}, \tag{10}$$

$$p_D\big|_{t_D=0} = 0, \tag{11}$$
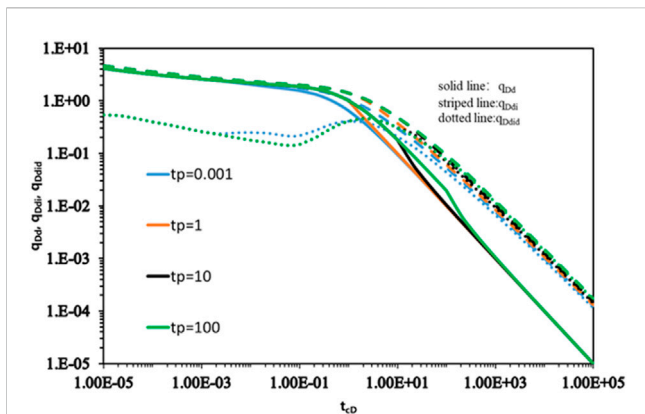
$$q_B = \frac{q_2}{q_i}, \tag{12}$$

FIGURE 6
Effect of Blasingame curves on P-2 delayed production from twin wells in circular homogeneous confined reservoirs producing at the same rate of constant production.

$$r_D \frac{\partial p_D}{\partial r_D}\Big|_{r_D=1} = -q_B, \tag{13}$$

$$\frac{\partial p_D}{\partial r_D}\Big|_{r_D=r_{eD}} = 0, \tag{14}$$

$$p_{2A} = p_D(r_1, t_D). \tag{15}$$

The dimensionless variables are defined as follows:

$$p_D(r_D, t_D) = \frac{kh}{1.842 \times 10^{-3} B q_i \mu}[p_i - p(r,t)], t_D = \frac{3.6kt}{\varnothing \mu C_t r_w^2},$$

$$r_w = \frac{r}{r_w}, \ r_{eD} = \frac{r_e}{r_w},$$

$$r_{eD2} = \frac{\int_0^{2\pi}\left[(r_{eD}\sin\theta)^2 + (r_{eD}\cos\theta + r_1)^2\right]d\theta}{2\pi},$$

where r is the distance from any point to the well in mm, r_w is the wellbore radius in mm, r_e is the drain radius in mm, k is the reservoir permeability in μm^2, θ is the reservoir porosity with no causality, C_t is the total reservoir compression factor in MPa^{-1}, h is the thickness of the reservoir in mm, μ is the viscosity of the crude oil in $MPa\cdot s$, B is a crude oil volume factor with no factorisation, q is the surface production of the well in m^3/d, p_i is the original stratigraphic pressure in MPa, p is the formation pressure at a point in the reservoir at a given time in MPa, and t is production time in h.

2.3 Solution of the mathematical model

A Laplace transformation of Eqs 5–15 yields

$$\frac{\partial^2 \tilde{p}_D}{\partial r_D^2} + \frac{1}{r_D}\frac{\partial \tilde{p}_D}{\partial r_D} = s\tilde{p}_D. \tag{16}$$

The boundary conditions within the P-1 well are expressed as

$$\frac{\partial \tilde{p}_D}{\partial r_D}\Big|_{r_D=1} = -\frac{1}{s}. \tag{17}$$

The boundary conditions within the P-2 well are expressed as

$$\frac{\partial \tilde{p}_D}{\partial r_D}\Big|_{r_D=1} = -\frac{q_B}{s}, \tag{18}$$

$$\frac{\partial \tilde{p}_D}{\partial r_D}\Big|_{r_D=r_{eD}} = 0. \tag{19}$$

Substituting Eq. 16 and Eq. 17 into Eq. 19, we have Eq. 20

$$\tilde{p}_{1A} = \frac{1}{s^{\frac{3}{2}}} \frac{K_0(\sqrt{s})I_1(r_{eD}\sqrt{s}) + I_0(\sqrt{s})K_1(r_{eD}\sqrt{s})}{K_1(\sqrt{s})I_1(r_{eD}\sqrt{s}) - I_1(\sqrt{s})K_1(r_{eD}\sqrt{s})}. \tag{20}$$

Substituting Eq.16 and Eq.18 into Eq. 19, we have Eq. 21

$$\tilde{p}_{2A} = \frac{q_B}{s^{\frac{3}{2}}} \frac{K_0(r_1\sqrt{s})I_1(r_{e1D}\sqrt{s}) + I_0(r_1\sqrt{s})K_1(r_{e1D}\sqrt{s})}{K_1(\sqrt{s})I_1(r_{e1D}\sqrt{s}) - I_1(\sqrt{s})K_1(r_{e1D}\sqrt{s})}. \tag{21}$$

Eq. 22 can be obtained from the Duhamel superposition principle:

$$\tilde{p}_A = \tilde{p}_{1A} + \tilde{p}_{2A}. \tag{22}$$

3 Plotting Blasingame-type curves

Plots of the rate solution q_D under a constant BHFP and the reciprocal of the pressure solution at a constant rate $(1/p_D)$ in the coordinate system are shown in Figure 3A. The figure indicates that the two curves almost overlap in the transient flow period and are dispersed in the boundary-dominated flow period. Palacio and Blasingame (1993) replaced dimensionless time t_D with dimensionless material balance time t_{cD} and plotted the above curves again. The result shows that the two curves overlap, as shown in Figure 3B. In other words, the solutions of variable flow rate and constant flow rate are equivalent due to the introduction of material balance time t_{cD}. Therefore, the Blasingame method is applicable to the condition of a variable BHFP and also to the condition of a variable flow rate (Liu, 2010; Yu, 2020).

3.1 Blasingame-type curve definitions of the dimensionless parameters

Blasingame-type curve definitions of the dimensionless parameters are formed by introducing normalisation coefficients, α, to the original definition of the dimensionless parameter.

Here, Blasingame-type curve definitions of the dimensionless parameters are as follows:

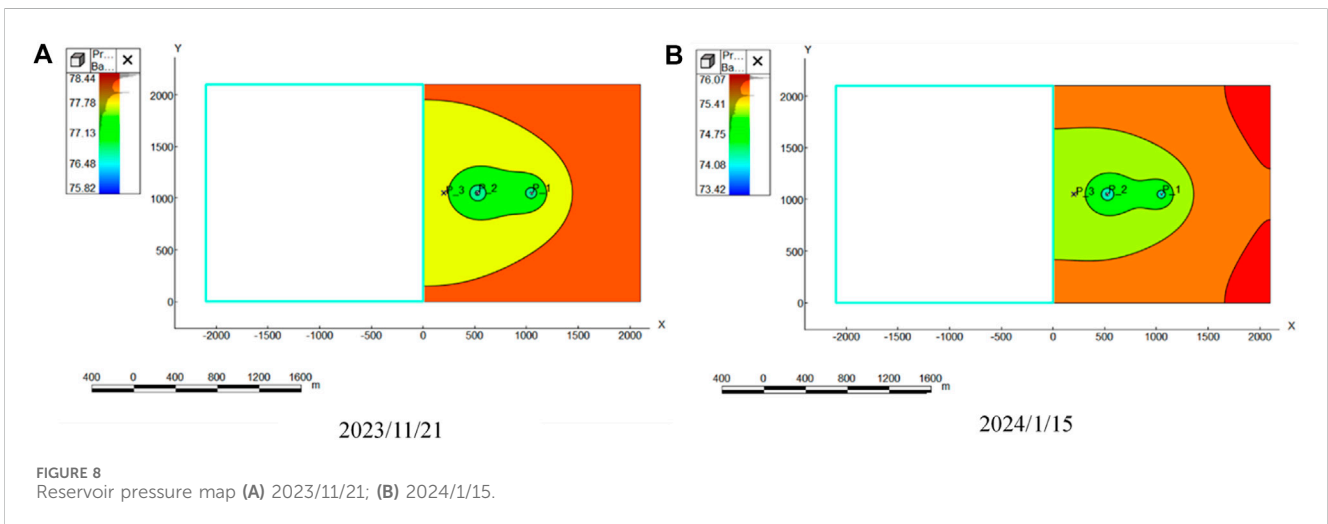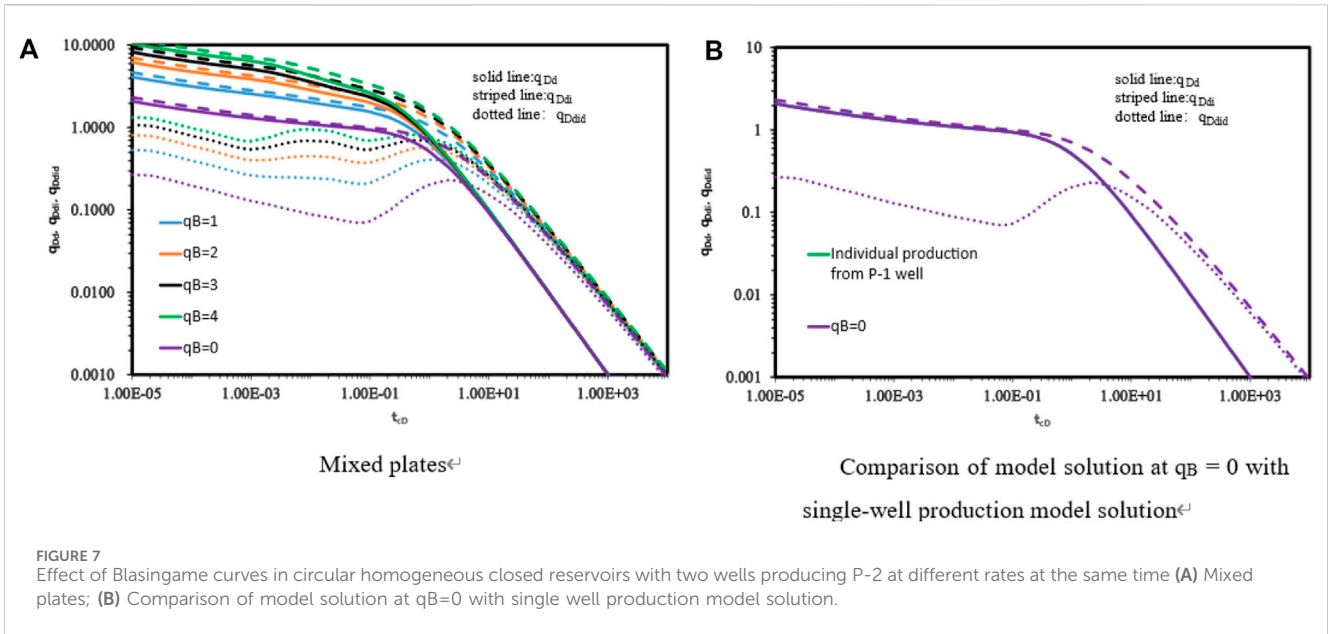Define the dimensionless material balance time as Eq. 23

$$t_{Dd} = \frac{1}{\frac{1}{2}(r_{eD}^2 - 1)\left(\ln r_{eD} - \frac{1}{2}\right)}t_D. \tag{23}$$

Define the dimensionless decline flow rate Eq. 24

$$q_{Dd} = \frac{(1 + q_B)\left(\ln r_{eD} - \frac{1}{2}\right)}{L^{-1}(\tilde{p}_A)}. \tag{24}$$

Define the dimensionless cumulative production as Eq. 25

$$N_{pDd} = \int_0^{t_{Dd}} q_{Dd}(\tau)d\tau. \tag{25}$$

FIGURE 7
Effect of Blasingame curves in circular homogeneous closed reservoirs with two wells producing P-2 at different rates at the same time **(A)** Mixed plates; **(B)** Comparison of model solution at qB=0 with single well production model solution.

FIGURE 8
Reservoir pressure map **(A)** 2023/11/21; **(B)** 2024/1/15.

Define the dimensionless decline flow rate integral function as Eq. 26

$$q_{Ddi} = \frac{\int_0^{t_{Dd}} q_{Dd}(\tau)d\tau}{t_{Dd}} = \frac{N_{pDd}}{t_{Dd}}. \quad (26)$$

Define the dimensionless decline flow rate integral derivative as Eq. 27

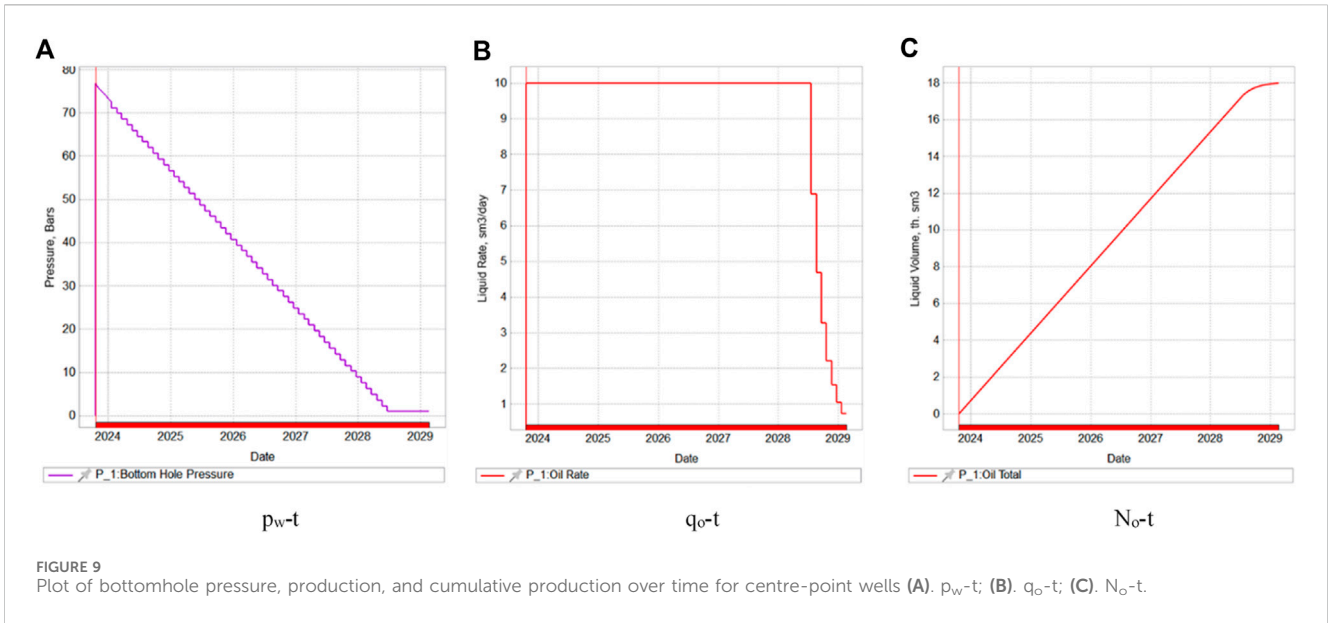$$q_{Ddid} = -\frac{dq_{Ddi}}{d\ln t_{Dd}} = q_{Ddi} - q_{Dd}. \quad (27)$$

3.2 Blasingame-type curves and model validation

Figure 4 shows an unstable analysis curve of production from double straight wells in homogeneous reservoirs. From Figure 4,

taking r_{eD} = 5,000 and q_B = 4 as an example, the crude oil flow can be roughly divided into an early radial flow stage, a stage influenced by the interference of neighbouring wells, and a later stage when the influence of the interfering wells is weakened (unsteady flow stage). The following section addresses the effect of well spacing, neighbouring well production, and neighbouring well start time factors on the Blasingame curve.

3.2.1 Effect of well spacing

Figure 5 shows the effect of different distances between two wells on the Blasingame curve when two wells in a circular homogeneous confined reservoir are producing at the same rate with simultaneous fixed production. From Figure 5, the early unstable flow stage of typical curves is a set of curves corresponding to different dimensionless well spacings, r_1. In the case of simultaneous production with the same yield, r_1 only affects the characteristics of the prior curve. When the pressure response from production from

FIGURE 9
Plot of bottomhole pressure, production, and cumulative production over time for centre-point wells **(A)**. p_w-t; **(B)**. q_o-t; **(C)**. N_o-t.

well P-2 has not yet reached point A, the curve is parallel to the curve when well p-1 is producing alone. When the pressure response from production in well P-2 reaches point A, inter-well interference occurs, and the regularised production curve begins to deviate downward. The larger the r_1, the greater the time for the material to begin to deviate from equilibrium, and the smaller the degree of t_{Dd} deviation, eventually converging in the boundary control flow stage into a straight line with a slope of −1, which corresponds to the characteristics of the curve of the proposed steady-state flow of the p-1 well when it is producing alone at a constant production rate $2q_i$. The variation in the integral curve with the regularised yield is similar to that of the regularised yield curve, which is grouped into a single curve at a later stage. For the regularised yield integral derivative curves, the inter-well disturbances during the unsteady seepage phase make them convex, and the larger r_1 is, the later the convexity appears, the lower and narrower the convexity is, and the later it is reduced to a single curve.

Let r_1 be 1; the two wells overlap as one well on the model, and the Blasingame type-curves coincide exactly with that of the single-well model. The correctness of the above dimensionless pressure-fitting regularised yield solution is proved.

3.2.2 Effect of well spacing

Figure 6 shows the effect of Blasingame curves on P-2 delayed production from twin wells in circular homogeneous confined reservoirs producing at the same rate of constant production. Typical curves are a set of curves corresponding to the different dimensionless material balance time delays of P-2 wells (with fixed production rates, denoted as q_i) during the opening of the well. For the same production rate and constant well spacing, the larger is t_p, the greater the time for downward deviation of the regularised production curve, which eventually converges into a straight line with a slope of −1 at the boundary control flow stage, corresponding to the curve characteristic of the proposed steady-state flow of the P-1 well when it is producing alone at a constant production rate of $2q_i$. For the regularised yield integral curve, the variation with t_p is similar to that of the regularised yield curve, but the larger t_p, the

later the curve is shifted upward in parallel. For the regularised yield integral derivative curves, inter-well disturbances during the unsteady seepage phase make them convex, and the larger t_p is, the later the convexity appears, the lower and narrower the convexity is, and the later curves are shifted upward in parallel.

3.2.3 Effect of production size of neighbouring wells

Figure 7 shows the effect of Blasingame curves in circular homogeneous closed reservoirs with two wells producing P-2 at different rates at the same time. Figure 7 shows that the type curves are a set of curves corresponding to the production of P-2 wells of different unfactored times. Under the condition of simultaneous production with the same well spacing, the larger q_B is, the higher the regularised production curve is, the smaller the time of downward deviation is, the larger the degree of deviation is, and finally, a straight line with a slope of −1 converges at the stage of boundary control flow. For the regularised yield integral curve, the variation with q_B is similar to that of the regularised yield curve, but the larger q_B, the later the curve is shifted downward in parallel. For the regularised yield integral derivative curve, the inter-well interference during the unsteady seepage phase makes it convex, and the larger q_B is, the faster the propagation of the pressure due to the production of the P-2 well is, the earlier the curve convexity appears, and the higher the convexity is.

Let $q_B = 0$. Only well P-1 is producing in the model, and the Blasingame curve of its model solution coincides exactly with that of the single-well model, that is, the correctness of the above dimensionless fitted-pressure regularised production solution is proved again.

4 Comparative analysis of numerical simulations

Figures 8, 9 show the reservoir pressure map and plot of the bottomhole pressure, production, and cumulative production over time for the centre point wells.

TABLE 2 Numerical simulation data—production data regularisation table.

Production date	P_1: Cumulative oil production, std m³	P_1: Wellbore pressure, bar	P_1: Daily oil production, std m³/d	t_{cD}	q_{Dd}
2023/10/19	0	0.0000	0		
2023/10/20	10	76.8691	10	1	3.91422
2023/10/21	20	76.6921	10	2	3.660608
2023/10/22	30	76.5706	10	3	3.504703
2023/10/23	40	76.4763	10	4	3.392629
2023/10/24	50	76.3982	10	5	3.305033
2023/10/25	60	76.3305	10	6	3.232691
2023/10/26	70	76.2698	10	7	3.170504
2023/10/27	80	76.2140	10	8	3.115385
2023/10/28	90	76.1617	10	9	3.065376
2023/10/29	100	76.1117	10	10	3.019178
2023/10/30	110	76.0636	10	11	2.975912
2023/10/31	120	76.0167	10	12	2.934966
		...			
2026/9/19	10,660	30.1731	10	1,066	0.203043
2026/10/19	10,960	28.8668	10	1,096	0.197796
2026/11/19	11,270	27.5167	10	1,127	0.192652
2026/12/19	11,570	26.2101	10	1,157	0.187921
2027/1/19	11,880	24.8599	10	1,188	0.183271
2027/2/19	12,190	23.5096	10	1,219	0.178845
2027/3/19	12,470	22.2898	10	1,247	0.175027
2027/4/19	12,780	20.9393	10	1,278	0.170985
2027/5/19	13,080	19.6322	10	1,308	0.167247
2027/6/19	13,390	18.2814	10	133	0.163552
2027/12/19	15,220	10.3054	10	1,522	0.144679
2028/1/19	15,530	8.9539	10	1,553	0.141904
2028/2/19	15,840	7.6023	10	1,584	0.139234
2028/3/19	16,130	6.3378	10	1,613	0.136825
2028/4/19	16,440	4.9860	10	1,644	0.13434
2028/5/19	16,740	3.6777	10	1,674	0.13202
2028/6/19	17,050	2.3257	10	1,705	0.129705
2028/7/19	17,350	1.0273	10	1,735	0.127557

From Figures 8, 9, tNavigator software was used to establish a 2000 m × 2000 m × 20 m reservoir 3-D model, with a grid step of 5 m, net-to-gross ratio of 0.1, porosity of 0.1, X-axis permeability of 100 mD, X-axis permeability of 100 mD, Z-axis permeability of 10 mD, an initial pressure of 80 MPa, a support depth of 110 m, a single-component model, a well at the centre point producing at a fixed rate, and another well at the grid coordinates (100, 100, 1) producing at the same rate, and two wells producing at the same time, and obtaining the data on the bottomhole pressure, the production rate, and the cumulative production rate of the wells at the centre point with the change of time.
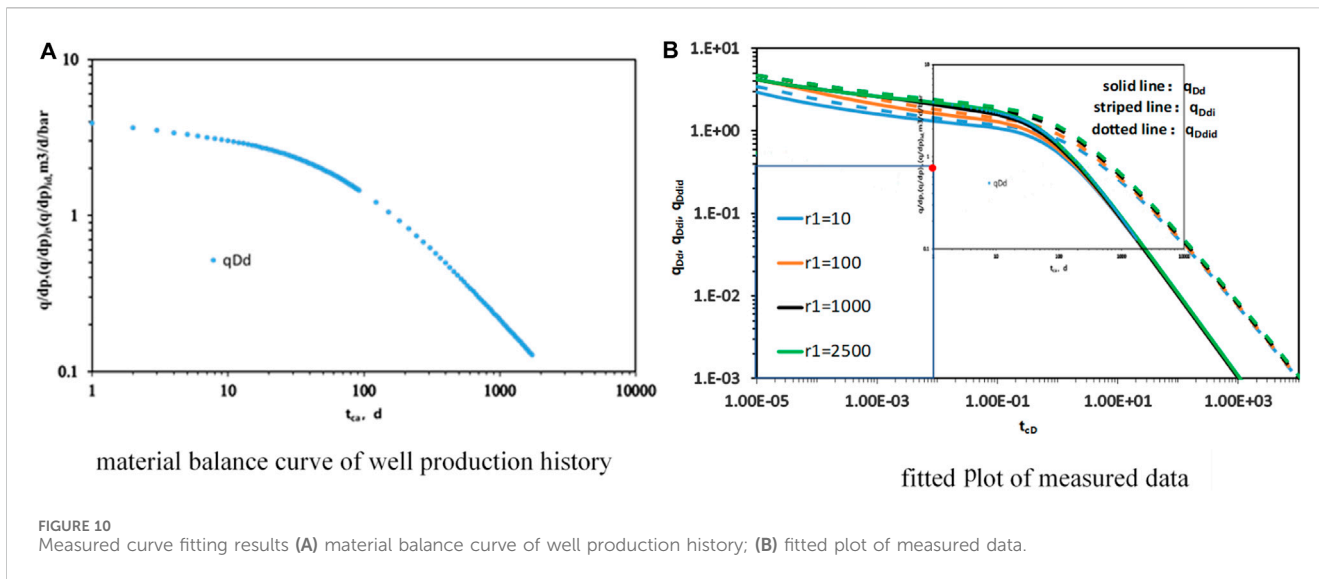
FIGURE 10
Measured curve fitting results **(A)** material balance curve of well production history; **(B)** fitted plot of measured data.
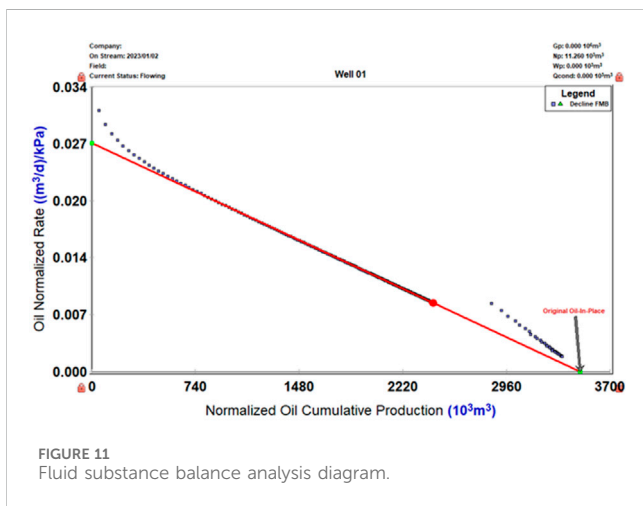

FIGURE 11
Fluid substance balance analysis diagram.

4.1 Data processing

To regularise the resultant data from numerical model runs, Calculate the material balance time by Eq. 28

$$t_c = \frac{N_p}{q}. \tag{28}$$

Calculate the normalised rate by Eq. 29

$$\frac{q}{\Delta p} = \frac{q}{p_i - p_{wf}}. \tag{29}$$

Calculate the normalised rate integral by Eq. 30

$$\left(\frac{q}{\Delta p}\right)_i = \frac{1}{t_c} \int_0^{t_c} \frac{q}{p_i - p_{wf}} dx. \tag{30}$$

Calculate the normalised rate integral derivative by Eq. 31

$$\left(\frac{q}{\Delta p}\right)_{id} = -t_c \frac{d\left(\frac{q}{\Delta p}\right)_i}{dt_c}. \tag{31}$$

Table 2 is the numerical simulation data–production data regularisation table.

4.2 Data fitting

Figure 10 shows measured curve fitting results from plotting the three relational curves, q_d-t_c, q_{di}-t_c, and q_{did}-t_c, fitting the Blasingame yield instability analysis plate, and recording the fitted values, where the three relational curves can be used simultaneously or individually.

Using the theoretical fit points $(8 \times 10^{-3}, 0.4)$, the actual fit points can be obtained $(1, 0.7)$.

The dynamic reserve at the centre point can be calculated according to the following Eq 32:

$$N = \frac{1}{C_t} \left(\frac{t_c}{t_{Dd}}\right)_M \left(\frac{q/\Delta p}{q_{Dd}}\right)_M (1 - S_w) \tag{32}$$

as 3.65×10^6 m³, and the numerical model has a reserve of 7.68×10^6 m³.

Additionally, the flowing material balance method (FMB) is listed for comparison to verify the accuracy of the method used in this article.

Figure 11 shows the equilibrium curves for the flowing material balance.

FMB is a method similar to the traditional material balance equation. However, it differs from the traditional material balance equation in that it uses dynamic pressure data instead of static pressure data for storage evaluation. Additionally, it differs from the flow material balance method, which uses flow pressure for dynamic storage evaluation. Once the reservoir is producing and has achieved a steady-state flow, the following relationship can be established (Eq. 33):

$$\frac{q}{\Delta p} = -\frac{N_p}{b_{pss} N \Delta p C_t} + \frac{1}{b_{pss}}. \tag{33}$$

The dynamic reserves N can be determined from the intercept results if the $\frac{q}{\Delta p} - \frac{N_p}{\Delta p C_t}$ curve is plotted.

From Figure 11, the dynamic reserves calculated for the P-1 well's reservoir are 3.486×10^6 m³. Comparing the results of the two methods, it is found that the method in this paper is more accurate in its calculations.

5 Conclusion

In this paper, the dual-well model is solved analytically by the equivalent well control radius method, and the following conclusions are reached:

(1) Based on establishing a constant production model that takes into account the effect of the presence of inter-well interference, the method of equivalent well control radius is used to simplify the treatment of the external boundary conditions of neighbouring wells that are not at the centre point of a circular closed reservoir. The range of applicability of the method is verified by comparing the equivalent well control surface with the actual well control area, and it is found that the method is more accurate when ($r_1 < 0.5r_{eD}$).

(2) Based on the method of equivalent well control radius, a sensitivity analysis of the Blasingame curve for the dual-well model can be conducted with respect to the parameters of adjacent well production, well spacing, and adjacent well opening time: the Blasingame normalised dimensionless decline flow rate integral curve is shifted downward when inter-well interference occurs, returning to a straight line later in the season. The Blasingame normalised dimensionless decline flow rate integral curve is shifted downward in the early stage, and the shape of the curve in the later stage is determined by the parameters. The Blasingame normalised dimensionless decline flow rate integral derivative curve has convex bulges, and the higher the degree of interference between the wells, the higher the bulges are, and the earlier they appear.

(3) Using the double-well production Blasingame curve plate for decreasing production analysis, the interpreted dynamic reserve results are more accurate for reservoirs with inter-well interferences, and the method in this paper can provide technical support for the fine evaluation of such reservoirs.

(4) Shortcomings: At present, the method is only applicable to analytical solutions and is used under the condition that r_1 (distance between wells) > r_{eD} (actual well control radius).

This is somewhat inapplicable to more complex models, such as composite media models, and requires further investigation.

Data availability statement

The original contributions presented in the study are included in the article/supplementary materials; further inquiries can be directed to the corresponding author.

Author contributions

PD: writing–original draft. QW: writing–review and editing. JZ: writing–review and editing. YW: writing–review and editing. DW: supervision and writing–review and editing. YH: software, supervision, and writing–review and editing. PL: validation and writing–review and editing.

Funding

Conflict of interest

The authors declare that the research was conducted in the absence of any commercial or financial relationships that could be construed as a potential conflict of interest.

Publisher's note

All claims expressed in this article are solely those of the authors and do not necessarily represent those of their affiliated organizations, or those of the publisher, the editors, and the reviewers. Any product that may be evaluated in this article, or claim that may be made by its manufacturer, is not guaranteed or endorsed by the publisher.

References

Alarji, H., Clark, S., and Regenauer-Lieb, K. (2022). Wormholes effect in carbonate acid enhanced oil recovery methods. *Adv. Geo-Energy Res.* 6 (6), 492–501. doi:10.46690/ager.2022.06.06

Chen, M., Wang, Z., Sun, H., Chang, C., Fuller, P. M., and Lu, J. (2017). Ventral medullary control of rapid eye movement sleep and atonia. *Petroleum Sci. Bull.* 2 (1), 53–62. doi:10.1016/j.expneurol.2017.01.002

Chen, Y. Q., Wang, X., and Liu, Y. (2023). The problems and derivation of Blasingame's steady-state pressure drop equation for variable production wells and its application. *J. China Offshore Oil Gas* 35 (6), 70–77. doi:10.2118/JCM-2023-35-6-070

Deng, Q., Nie, R., Jia, Y., Wang, X., Chen, Y., and Xiong, Y. (2015). "A new method of pressure buildup analysis for a well in a multi-well reservoir," in SPE North Africa Technical Conference and Exhibition, Cairo, Egypt, September 14-16, 2015.

Dong, J., and Zhai, Y. (1996). "Study on theoretical curve of well test under multi-well interference conditions," in Proceedings of the 5th National Symposium on Seepage Hydraulics SPE Asia Pacific Improved Oil Recovery Conference, Kuala Lumpur, Malaysia, October 25-26, 1999 (Beijing: Petroleum Industry Press), 188–193.

Gan, X., Yi, J., Ou, J., Yuan, Q., Deng, Z., Yan, P., et al. (2022). Numerical well test technology of gas well pressure recovery based on inter-well interference model. *Well Test. Oil Gas Wells* 31 (3), 9–15. doi:10.19680/j.cnki.1004-4388.2022.03.002

Guo, J., Ning, B., Yan, H., Jia, C., and Li, Y. (2022). Production performance analysis for deviated wells in carbonate gas reservoirs with multiple heterogeneous layers. *Front. Energy Res.* 10. doi:10.3389/fenrg.2022.861780

Jiang, R. Z., He, J. X., and Jiang Yu, F. H. (2019). Establishment and application of Blasingame's production decline analysis method for fractured horizontal wells in shale gas reservoirs. *Acta Pet. Sin.* 40 (12), 1503–1510. doi:10.7623/syxb201912009

Li, X., and Luo, J. (2009). Application research on the well test analysis model under the influence of adjacent wells. *Well Test.* 18 (2), 5–7. doi:10.3969/j.issn.1004-4388.2009.02.002

Lin, J., Liu, W., and Chen, Q. (1996). Application of the analysis theory of multi-well system for water injection development. *Petroleum Explor. Dev.* 23 (3), 58–63.

Lin, J., and Yang, H. (2005b). Pressure buildup analysis for a well in a closed, bounded multi-well reservoir. *Chin. J. Chem. Eng.* 13 (4), 441–450. doi:10.1002/cite.200590223

Lin, J., and Yang, H. (2007). "Analysis of well-test data in a multi-well reservoir with water injection," in SPE Annual Technical Conference and Exhibition, Anaheim, California, November 11-14, 2007.

Liu, Q., Chen, Y., Zhang, L., and Wang, W. (2006). Study on the model and interpretation method of interference well testing without shutting in. *Well Test.* 15 (1), 10–12. doi:10.3969/j.issn.1004-4388.2006.01.004

Liu, X., Zou, C., Jiang, Y., and Yang, X. (2010). Basic principles and applications of modern production decline analysis. *Nat. Gas. Ind.* 30 (5), 50–54. doi:10.3787/j.issn.1000-0976.2010.05.012

Liu, Y., Chen, H., Zhang, D., Zhou, R., and Liu, Y. (2002). Numerical well test analysis of oil wells under the condition of adjacent well influence. *Well Test.* 11 (5), 4–7. doi:10.3969/j.issn.1004-4388.2002.05.002

Liu, Y., Jia, Y., Kang, Y., and Huo, J. (2008). A survey of genetic simulation software for population and epidemiological studies. *Drill. Prod. Technol.* 31 (1), 79–86. doi:10.1186/1479-7364-3-1-79

Li, S., Zhou, R., and Huang, B. (1994). Theoretical analysis and application of interference pressure among adjacent wells. *Petroleum Explor. Dev.* 1 (1), 84–88. 128.

Mccray, T. L. (1990). *Reservoir analysis using production decline data and adjusted time.* United States: Texas A&M University.

Onur, M., Serra, K. V., and Reynolds, A. C. (1991). Analysis of pressure buildup data from a well in a multi-well system. *SPE Form. Eval.* 6 (1), 101–110. doi:10.2118/18123-pa

Palacio, J. C., and Blasingame, T. A. (1993). *Decline-curve analysis using type curves analysis of gas well production data. SPE 25909.*

Pang, J., Lei, G., Liu, H., and Zhang, X. (2012). Evaluation of well-to-well interference in gas wells using the material balance method. *Sci. Technol. Eng.* 12 (26), 6787–6789. 6793. doi:10.3969/j.issn.1671-1815.2012.26.049

Spivey, J. P., and John Lee, W. (2016). *Practical well test interpretation methods, translated by yongxin han, H Sun, xg Deng, and Y shi.* Beijing: Petroleum Industry Press.

Sun, H. (2005). *Advanced production decline analysis and application.* Oxford: Gulf Professional Publishing.

Sun, H. (2013). *Modern production decline analysis method and application of oil and gas wells.* Beijing: Petroleum Industry Press.

Sun, H. (2015). *Advanced production decline analysis and application.* Gulf Professional Publishing.

Sun, H. (2016). Analysis method of multi-well pressure recovery well test under the condition of adjacent well interference. *Nat. Gas. Ind.* 36 (5), 62–68. doi:10.3787/j.issn.1000-0976.2016.05.009

Wang, F. (2015). Diagnosis of nonlinear reservoir behaviour for correctly applying the superposition principle and deconvolution. *J. Nat. Gas Sci. Eng.* 26, 630–641. doi:10.1016/j.jngse.2015.07.004

Wang, Y., Dai, Z., Chen, Li, Shen, X., Chen, F., and Soltanian, M. R. (2023). An integrated multi-scale model for CO2 transport and storage in shale reservoirs. *Appl. Energy* 331, 120444. doi:10.1016/j.apenergy.2022.120444

Wang, Y.-W., and Dai, Z.-X. (2023). A hybrid physics-informed data-driven neural network for CO2 storage in depleted shale reservoirs. *Petroleum Sci.* 16 (1), 109–120. doi:10.3969/j.issn.1000-9585.2023.01.014

Wei, C., Cheng, S., Bai, J., Li, Z., Shi, W., Wu, J., et al. (2022b). Analytical well test analysis method for finite conductivity fractured well under multi-well interference. *Petroleum Geol. Oilfield Dev. Daqing* 41 (4). doi:10.19597/J.ISSN.1000-3754.202103018

Wei, C., Cheng, S., Jiang, B., Li, Z., Shi, W., Wu, J., et al. (2022a). Analytical well test analysis method for finite conductivity fractured wells under multi-well interference. *Daqing Petroleum Geol. Dev.* 41 (4), 90–97. doi:10.19597/J.ISSN.1000-3754.202103018

Xu, Y., Liu, Q., Xiaoping, Li, Wang, X. J., Liang, H. S., Zeng, Z. C., et al. (2021). Fbf1 regulates mouse oocyte meiosis by influencing Plk1. *Nat. Gas. Ind.* 41 (6), 74–83. doi:10.1016/j.theriogenology.2021.01.018

Yu, Q., Hu, X., Li, Y., and Jia, Y (2020). Dynamic evaluation method of oil well parameters and reservoir parameters in drilling large caves. *Oil Gas Geol.* 41 (3), 647–654. doi:10.11743/ogg20200320

Zeng, T., Jia, Y., Wang, H., Tang, D., and Zhang, W. (2006). Analysis of the finite multi-well system well test model and template curve. *Xinjiang Pet. Geol.* 27 (1), 86–88. doi:10.3969/j.issn.1001-3873.2006.01.024

Zeng, Y., Kang, X., Tang, E., Liang, D., and Cheng, S. (2020). A new well test interpretation model for injection polymer wells considering adjacent well interference. *J. Chengdu Univ. Technol. Sci. Technol. Ed.* 47 (1), 85–91. doi:10.3969/j.issn.1671-9727.2020.01.08

Zhang, L., Xiang, Z., Li, Y., Li, X., and Liu, Q. (2006). Impact of well-to-well interference on oil-water two-phase flow numerical well test curves. *J. Hydrodynamics Ser. A* 21 (6), 805–810.

Zhang, X., Jia, Y., Yan, T., Peng, H., Wergedal, J. E., Guttierez, G. G., et al. (2004). Local *ex vivo* gene therapy with bone marrow stromal cells expressing human BMP4 promotes endosteal bone formation in mice. *Well Test. Technol.* 25 (3), 4–15. doi:10.1002/jgm.477

Zhao, J., Wang, L., Liu, S., Kang, Z., Yang, D., and Zhao, Y. (2022). Numerical simulation and thermo-hydro-mechanical coupling model of *in situ* mining of low-mature organic-rich shale by convection heating. *Adv. Geo-Energy Res.* 6 (6), 502–514. doi:10.46690/ager.2022.06.07

Zhou, S., Wang, H., Li, B., Li, S., Sepehrnoori, K., and Cai, J. (2022). Predicting adsorbed gas capacity of deep shales under high temperature and pressure: experiments and modeling. *Adv. Geo-Energy Res.* 6 (6), 482–491. doi:10.46690/ager.2022.06.05